Internal Energy Transfer in Laser Desorption/Ionization from Silicon Nanowires

5 **AUTHORS**, INCLUDING:

Akos Vertes
George Washington University

194 PUBLICATIONS   **4,625** CITATIONS

Internal Energy Transfer in Laser Desorption/Ionization from Silicon Nanowires

Guanghong Luo,[†] Yong Chen,[†] Hugh Daniels,[‡] Robert Dubrow,[‡] and Akos Vertes*,[†]

Department of Chemistry, Institute for Proteomics Technology and Applications, The George Washington University, Washington, DC 20052, and Nanosys, Inc., 2625 Hanover Street, Palo Alto, California 94304

Received: February 14, 2006; In Final Form: May 12, 2006

Laser-induced desorption/ionization from silicon nanowires (SiNW) is an emerging method for mass spectrometry of small to medium-size molecules. In this new technique, we examined the internal energy transfer to seven benzylpyridinium thermometer ions and extracted the corresponding internal energy distributions. To explore the effect of the energy-deposition rate on the internal energy transfer, two lasers with significantly different pulse lengths (4 ns vs 22 ps) were utilized as excitation sources. A comparison of ion yields indicated that the SiNW substrates required 5−8 times less laser fluence for ion production than either matrix-assisted laser desorption/ionization (MALDI) or desorption/ionization on silicon (DIOS). In contrast however, the survival yield (SY) values showed that the internal energy transferred to the thermometer ions was more than (ps laser) or comparable to (ns laser) MALDI but it was significantly less than in DIOS. The internal energy transfer was only slightly dependent on laser fluence and on wire density. These effects were rationalized in terms of the confinement of thermal energy in the nanowires and of unimpeded three-dimensional plume expansion. Unlike in MALDI from CHCA and in perfluorophenyl-derivatized DIOS, for desorption from SiNWs the effect of laser pulse length on the internal energy transfer was found to be negligible.

Introduction

For the mass spectrometric investigation of small- to medium-sized molecules, nanostructured surfaces offer an effective alternative for the organic matrixes used in matrix-assisted laser desorption/ionization (MALDI). The main drawback of MALDI for these analytes is that through spectral interferences the ions derived from the matrix obscure their mass spectra. Following the landmark discovery of cobalt nanoparticles for soft laser desorption/ionization (SLDI) in the late 1980s,[1] various materials have been investigated for their potential as desorption/ionization substrates. Diverse classes of micro- and nanoparticles were shown to be efficient for the SLDI of peptides and proteins.[2−5] Recently, small nanoparticles (2−5 nm in diameter) with possible quantum confinement effects were demonstrated to generate peptide ions.[6] Nanotubes[7,8] and nanostructured films[9] were also proven to function as SLDI substrates.

Desorption/ionization on porous silicon (DIOS) represents a particularly efficient SLDI method.[10] To date, DIOS has been successfully applied in the analyses of small molecules, pharmaceuticals, peptides, small proteins, synthetic polymers, and enzymes.[11−14] Efficient ion production in DIOS is generally attributed to the special properties of porous silicon, including its high surface area, thermal conductivity, UV absorptivity, and its ability to trap solvent or residual gas molecules. Additionally, changes in the doping and morphology of porous silicon have the potential to broaden the selection of excitation sources beyond the currently common UV lasers.[15]

Silicon nanowires (SiNWs) are quasi-one-dimensional systems with unique optical and surface properties that make them promising candidates as SLDI substrates.[16] SiNWs can be synthesized by gold nanoparticle-catalyzed vapor−liquid−solid deposition that allows for the delicate control of physical dimensions, composition, and density at the nanoscopic level.[17] These properties, in turn, directly affect the optical, thermal, and surface properties of the nanowires. The high surface area of SiNW promotes adsorption and accumulates the sample or solvent molecules. When the incident laser beam excites the quantum-confined electrons in the SiNWs, it sharply increases the surface temperature and induces desorption. Through these systems, correlations between the SiNW physical properties and the SLDI pathways can be explored.

Because of the one-dimensional structure of SiNWs, their optical and thermal properties are significantly altered compared to those of bulk silicon. The bulk band gap, $E_g = 1.1$ eV, of silicon rapidly increases at small diameters, d, and large aspect ratios, $L/d \gg 1$, where L is the length of the wire, but this change only becomes noticeable below $d = 2.2$ nm.[18,19] Thus, the nanowires in this study with $d = 40$ nm are expected to retain the optical properties of bulk silicon. The thermal conductivity at room temperature, κ, however, does drop for these nanowires from the bulk value of $\kappa_b = 148$ W/mK to ∼20 W/mK.[20] This is primarily attributed to the increased phonon-boundary scattering in the nanowires.[21] The bulk thermal conductivity also diminishes with increasing temperature: close to the 1687 K melting point (e.g., at 1600 K), it reduces to ∼22 W/mK. Although there are no thermal conductivity measurements on SiNWs at elevated temperatures, one expects further reduction by approximately another order of magnitude.

Upon laser irradiation of SiNWs in a desorption experiment, the heat dissipation through conduction is arrested because of the decreased conductivity and the thermal confinement in the nanowires.[22] Compared to macroscopic targets, this leads to elevated surface temperatures on these structures, or conversely, for SiNWs, a lower laser fluence is sufficient to reach the same surface temperature as a macroscopic target. Furthermore, at

* To whom correspondence should be addressed. E-mail: vertes@gwu.edu. Phone: (202) 994-2717. Fax: (202) 994-5873.
† The George Washington University.
‡ Nanosys, Inc.

length scales smaller than the phonon mean free path, λ, which can be expressed as $\lambda = 3\kappa/(C_v c)$ where $C_v = 19.8$ J/mol K is the volumetric heat capacity and $c = 4500$ m/s is the sound velocity in silicon, the Fourier heat conduction equation has to be replaced by the ballistic-diffusive heat transport equation.[23,24] The phonon mean free path in SiNWs at 300 K is $\lambda \approx 800$ nm, which is much longer than the diameter of the nanowires in this study. Thus, the role of ballistic heat transport cannot be neglected.

In a previous report, we introduced dense arrays of single-crystal SiNWs as a platform for SLDI mass spectrometry.[16] In that investigation, preliminary data indicated that SLDI from SiNW required much lower laser fluence than MALDI or DIOS. To further explore the energy transfer in laser desorption from this nanostructure, in the present study, we systematically investigate the internal energies for a series of thermometer ions using two different laser excitation sources.

The internal energy transfer is a crucial parameter that determines fragmentation and metastable decay in soft ionization methods. Moreover, internal energy transfer data can provide insight into the fundamental mechanisms controlling these processes. Investigations of the internal energy transfer in soft ionization methods such as electrospray ionization (ESI) and MALDI have contributed to the understanding of these two techniques.[25-30] It is expected that internal energy transfer during SLDI from SiNWs can help to clarify the mechanism of this new method.

In this study, we investigated the effect of laser pulse length, laser fluence, and to a certain extent, surface morphology (i.e., wire density) on the internal energy transfer in SLDI from SiNWs. Seven benzyl-substituted benzylpyridinium thermometer ions were utilized to gauge the energy content of the desorbed species through their survival yields.

Experimental Section

Synthesis of SiNWs and Surface Derivatization. The SiNWs used in this study were synthesized by the vapor−liquid−solid growth technique.[17] Size-selected colloidal gold particles were deposited on silicon wafers by spin-coating. After elimination of the solvents and organic residues, the substrates were placed in a 480 °C chemical vapor deposition furnace to grow the SiNWs with silane (SiH$_4$) as the vapor-phase reactant. The produced SiNWs were ∼40 nm in diameter and a few micrometers long with a density of 10−50 wires/μm^2. To decrease the density to <10 wires/μm^2, abraded SiNW surfaces were prepared by placing another silicon wafer on top of the nanowires and sliding it in one direction.

For derivatization, the SiNWs were first etched in 5% HF solution to remove the oxide layer and then reoxidized with ozone. The oxidized surfaces were subsequently treated with a silylating reagent, (pentafluorophenyl)-propyldimethylchlorosilane (Gelest, Inc., Morrisville, PA), to produce the perfluorophenyl (PFP) derivatized surfaces. The detailed silylation procedures are described in ref 16. After the surface modification, the SiNWs were rinsed with methanol and dried in a stream of pure N$_2$.

Surface Characterization. Before and after the laser desorption experiments, a scanning electron microscope (SEM) (LEO 1460VP, Carl Zeiss, Thornwood, NY) was used to examine the surface morphology. Amplification and focusing conditions were optimized for each sample.

Mass Spectrometry. The home-built time-of-flight (TOF) mass spectrometer and the methods for studying thermometer ions were presented elsewhere.[29] In brief, the spectrometer includes a laser desorption ion source with two alternative lasers and a 2.1 m linear flight tube. The ions were accelerated by 25 kV from the SLDI source into a field-free region, and after separation according to their flight time, they were detected by a dual multichannel plate assembly. The signal was amplified by a preamplifier and transmitted to a fast digital oscilloscope. A custom-made LabVIEW program was used for data acquisition and evaluation on a PC platform. The MALDI sample probe was modified to accommodate the SiNW surface.

Chloride salts of seven benzyl-substituted benzylpyridinium ions (with 2-methyl (2M), 3-methyl (3M), 4-methyl (4M), 3-methoxy (3MO), 4-methoxy (4MO), 4-chloro (4C), and 4-fluoro (4F) substituents, respectively) were dissolved in 50% methanol (v/v) at a concentration of ∼70 μM. For sample preparation, 0.5 μL of this solution was deposited on the SiNW substrate and dried under ambient conditions. The SiNW surfaces were attached to the stainless steel solid insertion probe by conductive double-sided carbon tape. Statistically sound data was collected and survival yield (SY) values, $SY = I(M^+)/(I(F^+) + I(M^+))$, were calculated for the thermometer ions.

Laser Sources. To explore the effect of the energy deposition rate on the internal energy transfer in SLDI from SiNW, two different lasers were utilized. The ion yields produced by a nitrogen laser with a wavelength of 337 nm and 4 ns pulse length (VSL-337ND, Laser Science Inc., Newton, MA) or alternatively by a mode locked $3 \times \omega$ Nd:YAG laser with a wavelength of 355 nm and 22 ps pulse length (PL2143, EKSPLA, Vilnius, Lithuania) were recorded in a fluence range starting from the ion fragmentation threshold for each sample. A low-pass optical filter was implemented in the ps laser beam path to reject the possible bleeding of the second harmonic (532 nm) in the 355 nm output. Both lasers were operated at a 2 Hz repetition rate.

Internal Energy Distributions. The dependence of SYs on the critical energy,[25,31] E_0, of the various thermometer ions was plotted for comparable laser fluence levels. The data sets were fitted with a Boltzmann-type sigmoidal curve, $SY = 1 - [1 + \exp(E_0 - E^*)/\Delta E]^{-1}$, where E^* was the center and ΔE was the width of the distribution. The squared correlation coefficient, R^2, was consistently larger than 0.98. For a specific combination of laser and SiNW surface, the derivative of this curve represented the internal energy distribution without the kinetic shift.

Results and Discussion

Morphology of SiNW Surface. A SEM image of the PFP derivatized SiNW surface before laser exposure is shown in Figure 1. The surface is covered by an entangled network of SiNWs that have individual diameters of ∼40 nm and lengths of several micrometers. The bright spots on the tip of these SiNWs are the gold seed particles. On the abraded samples, SiNWs were partially removed until the wire density decreased to < 10 wires/μm^2. As a consequence, the images for these surfaces were of lesser quality. At elevated laser fluence levels, patches of the exposed nanowires were missing, pointing to likely ablation damage of the SiNWs. However, the silicon ablation indicated by these images did not result in the appearance of related ions.

Survival Yields from SiNWs. The SYs of seven thermometer ions were used to gauge the internal energy transfer from PFP derivatized SiNW surfaces. In Figure 2 we plotted the SYs of 4M ions desorbed from the SiNW surface together with the data from a PFP-derivatized DIOS surface and from an α-cyano-4-hydroxycinnamic acid (CHCA) MALDI matrix. Figure 2 indicates that the 4 mJ/cm^2 fluence threshold (ns laser) for

Laser Desorption/Ionization from Silicon Nanowires

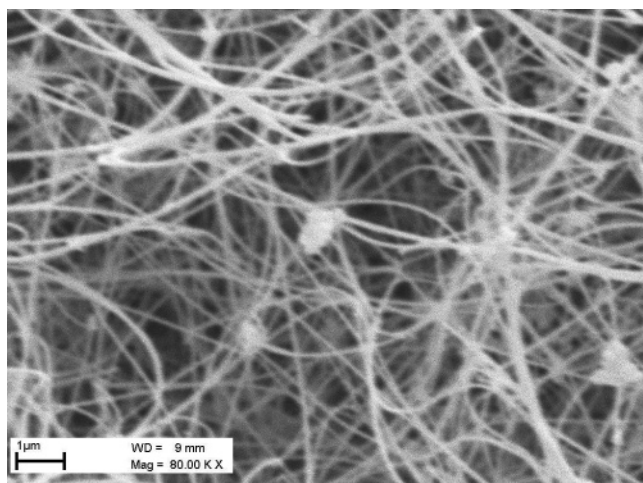*J. Phys. Chem. B, Vol. 110, No. 27, 2006* **13383**

Figure 1. SEM image of ~40 nm diameter native PFP-derivatized SiNWs used as desorption/ionization substrate.
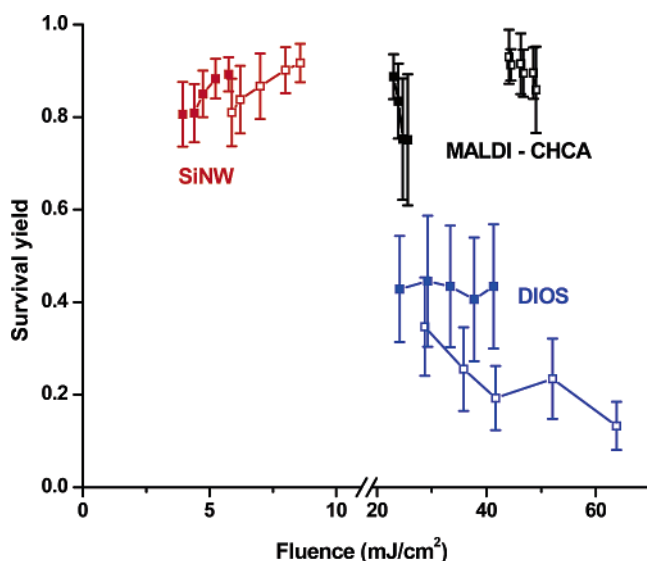

Figure 2. Comparison of survival yields of 4M benzylpyridinium ions in desorption/ionization from SiNWs, DIOS, and MALDI. Desorption/ionization from SiNWs required significantly lower laser fluence than the other two methods. All solid symbols are for the nanosecond laser, and all hollow symbols are for the picosecond laser: (red) PFP-derivatized SiNW surface, (blue) PFP modified DIOS, and (black) MALDI from CHCA matrix.

detectable ion production from the SiNW is dramatically lower than the corresponding values for either DIOS or MALDI (both of them are ~24 mJ/cm^2). For the ps laser, the SiNWs require 6 mJ/cm^2, whereas the threshold fluences for DIOS and MALDI are 29 mJ/cm^2 and 44 mJ/cm^2, respectively.

The 5−8 times lower laser energy required for SLDI on the SiNW surface can be attributed to the unique geometry and thermal properties of the SiNWs. Assuming that the SiNWs have a similar absorption coefficient to bulk silicon, the laser penetration depth at 337 nm wavelength is ~10 nm[32] (i.e., one-quarter of the SiNW diameter). Thus, deposition of laser energy in the SiNWs can be treated as a penetrating source in a slender cylindrical absorber. Because of the small diameter of the cylinder, the heat conduction is confined and the energy can only dissipate in the axial direction. This confinement of thermal energy is more profound but similar to the problem of laser energy deposition in thin films. When the smallest dimension of an object (e.g., the thickness of a thin film) becomes comparable to the heat conduction length, energy dissipation

through heat conduction is obstructed and the maximum surface temperature of the object increases dramatically. For example, it is known that small crystallites (~1 μm) in MALDI undergo explosive evaporation, whereas larger ones gradually reduce in size.[22,33] In SiNWs, this effect is further exacerbated by the reduced thermal conductivity because of the small diameter and elevated temperature. As a consequence, during desorption/ionization from SiNW, compared to bulk targets, much lower laser fluences are sufficient to rapidly raise the surface temperature and trigger desorption.

Another interesting observation in Figure 2 is that the absolute value of the SYs in desorption/ionization on SiNW is comparable to MALDI. Even though the SiNWs require much lower laser fluence for ion production than the CHCA matrix, the SY values for both methods are in the 0.8−0.9 range. Similar SYs indicate similar internal energy transfer during the desorption. This means that the surface temperatures on SiNWs reach similar values to the temperatures experienced in MALDI already at a much lower fluence level. Because of the reduced thermal conductivity in the hot SiNWs, these temperatures are sustained for a longer period than they would be on the surface of bulk silicon. The energy exchange between the surface and the thermometer ions is limited by the finite interaction time defined by the departure of the adsorbates from the surface.

Compared to another nanostructure, the nanoporous silicon in DIOS, the SYs for desorption from SiNW are much higher. For example, for the nanosecond laser, the DIOS SYs are ~0.4, whereas the SiNW values are at 0.8 and higher. This difference can be attributed to the different dimensionality of plume expansion.[34] While for SiNW the expansion of the desorbed plume is three-dimensional, for the nanopores in DIOS the plume expansion is quasi-one-dimensional. The confinement of the DIOS plume in the nanopores results in more efficient energy transfer than in the three-dimensional unobstructed expansion for SiNWs.

An interesting observation in Figure 2 is the apparent slight increase of SYs with the laser fluence. This unexpected trend is in contrast to our observations for MALDI and, to some extent, for DIOS. In MALDI, the SY for desorption from CHCA matrix shows a sharp drop with increasing laser fluence. In DIOS, the SY as a function of fluence is practically unchanged for the nanosecond laser and shows moderate decline for picosecond laser. The counterintuitive weakly increasing trend observed for SiNWs may be considered an artifact because of the onset of silicon melting and ablation at fluences above the corresponding threshold.

Comparison of PFP-Derivatized and Abraded Surfaces. To explore the effect of nanowire density, some of the SiNWs were removed by abrasion. Figure 3 illustrates the correlation of SY with the laser fluence and laser pulse length for two representative thermometer ions (4MO and 4M) on PFP-derivatized (with 10−50 wires/μm^2) (solid symbols) and abraded (with less than 10 wires/μm^2) (hollow symbols) SiNW surfaces. In all cases, relatively low laser fluence was sufficient for ion production. While for the picosecond laser pulses, an approximately 1.5 times higher fluence was needed than for nanosecond laser excitation; the SYs were similar.

The differences between the native PFP-derivatized and abraded (low density) nanowire systems were fairly minor. Consistently higher threshold fluences were observed for the lower wire density. Compared to the denser native SiNW surface, at a similar fluence, the abraded SiNWs exhibited slightly lower average SY values. Both of these observations are consistent with the role the SiNWs play in the energy
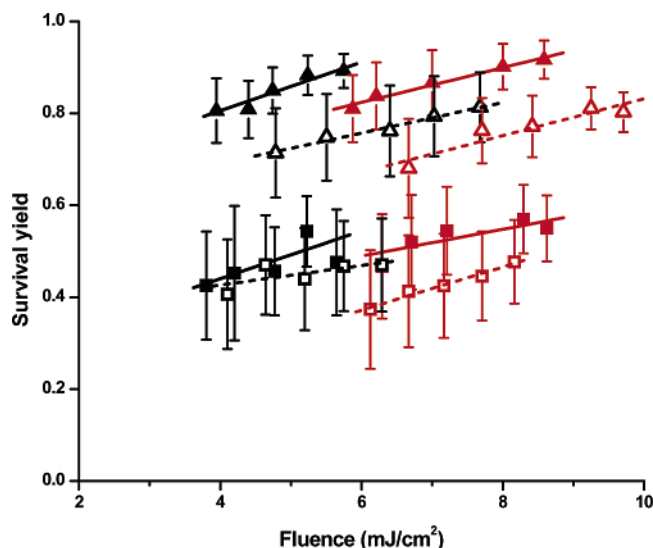
Figure 3. Survival yields of representative benzylpyridinium thermometer ions desorbed from native PFP derivatized SiNW surface with 10−50 wires/μm^2 (solid symbols) and abraded SiNW surface with <10 wires/μm^2 (hollow symbols). For both surfaces the following symbols are used: (black ■ and □) 4MO with nanosecond laser, (red ■ and □) 4MO with picosecond laser, (black ▲ and △) 4M with nanosecond laser, and (red ▲ and △) 4M with picosecond laser.

deposition process. Having less of the wires per unit area on the surface means a lower occurrence of enhanced rapid heating from the energy confinement in the wires. Thus, a higher fluence is needed to reach the same surface temperature, hence the higher threshold fluence, and higher internal energy transfer takes place, hence the lower SY.

Consistent with the results for 4M thermometer ions with increasing laser fluence, for the other species in Figure 3, the SY value slightly increases. The slopes of the linear fits in Figure 3 for the PFP-derivatized surfaces are 0.052 ± 0.032 (4MO) and 0.053 ± 0.009 cm^2/mJ (4M) for the nanosecond laser and 0.029 ± 0.012 (4MO) and 0.038 ± 0.003 cm^2/mJ (4M) for the picosecond laser. This is an apparent departure from the observations in SLDI and in laser ablation and in fact contradicts the general nature of breakdown curves. It is expected that with increasing internal energy the relative abundance of a precursor ion declines and fragment ions appear (see for example, ref 35).

Assuming that increased fluence levels result in higher internal energy, one would expect the SY to be constant up to the breakdown where it should drop precipitously. The data in Figure 3 does not follow this pattern, instead, with increasing fluence there is a slight increase in the SYs. In only a few cases (the 4MO ion with both lasers), we see a slight downturn of SYs at the highest measured fluences. This observation points to a very limited change in the internal energy as the laser fluence increases. Similar to the case of DIOS, although in a much narrower fluence range, the lack of decline in SY for the SiNW substrates can be attributed to the arrested energy exchange between the hot surface and the desorbed analyte because of the departure of the latter. In contrast, in a MALDI plume, the hot matrix material expands together with the desorbed ions, which results in prolonged energy exchange.

The reduced interaction time, however, does not give an explanation for the slight increase in the SYs. As mentioned earlier, we consider this an artifact probably linked to the onset of SiNW evaporation. SEM images of the SiNW surfaces following the laser desorption experiments indicate that in the areas exposed to higher fluences the SiNWs were missing (Figure 4). This observation points to the ablation of the
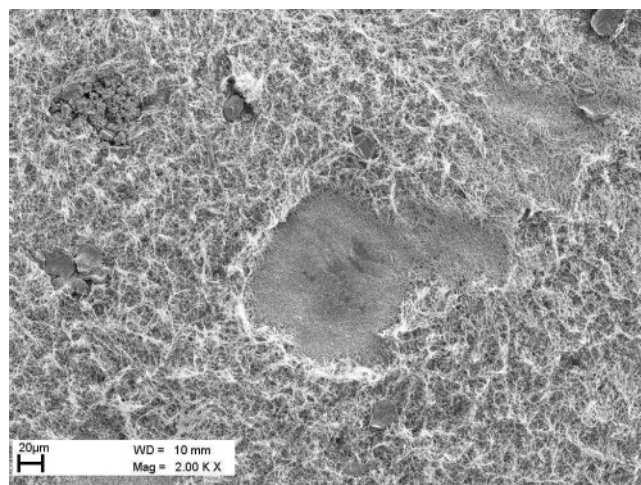

Figure 4. After laser desorption experiments at elevated fluences, SEM image of native SiNW surface indicates removal of nanowires from high fluence area. Only moderate damage of the underlying flat silicon surface is observed.
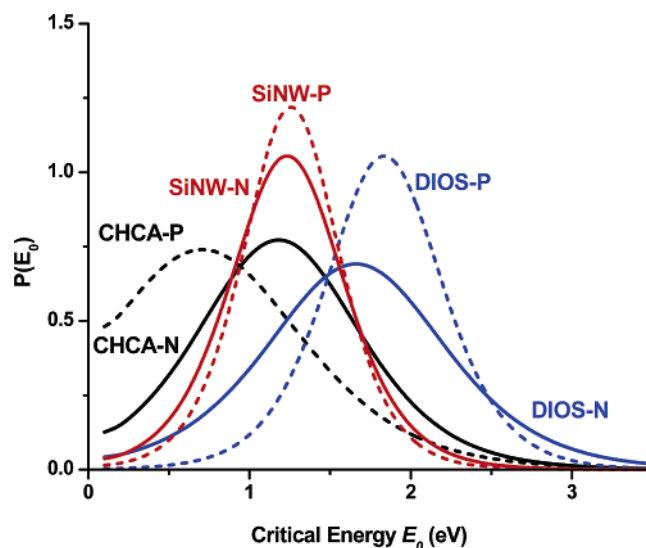

Figure 5. Internal energy distributions of benzylpyridinium ions desorbed from native PFP-derivatized SiNW surface, PFP-modified DIOS, and MALDI from CHCA matrix. Solid lines represent results with the nanosecond laser, whereas dashed lines indicate picosecond laser excitation. The following labels are used in the figure: CHCA-N, CHCA with the nanosecond laser; CHCA-P, CHCA with the picosecond laser; DIOS-N, DIOS surface with the nanosecond laser; DIOS-P, DIOS surface with the picosecond laser; SiNW-N, SiNWs with the nanosecond laser; and SiNW-P, SiNWs with the picosecond laser.

nanowires. Because of the confinement of thermal energy, the ablation of the nanowires is expected to happen significantly below the ablation threshold for bulk silicon. This is confirmed by the SEM image in Figure 4, as there is very limited ablation damage on the flat silicon surface where the nanowires are removed.

Internal Energy Distributions. Because the seven thermometer ions represent a wide range of the critical energies, 1.34 < E_0 < 2.20 eV, the distribution of the internal energies (in addition to the mean values) can also be extracted from the SY measurements.[25,26] At a selected F fluence, SY values were collected for all thermometer ions using the nanosecond and the picosecond lasers. Figure 5 shows a comparison of the internal energy distributions obtained from three SLDI methods, desorption/ionization from SiNWs, MALDI from CHCA matrix,

Laser Desorption/Ionization from Silicon Nanowires

J. Phys. Chem. B, Vol. 110, No. 27, 2006 **13385**

TABLE 1: Internal Energy Distribution Characteristics in MALDI, DIOS, and Desorption from Native PFP-Derivatized SiNWs

laser sources	methods	F (mJ/cm^2)	E^* (eV)	ΔE (eV)	R^2
nanosecond	DIOS−PFP	40.7	1.66 ± 0.13	0.37 ± 0.20	0.91
	SiNW−PFP	5.22	1.23 ± 0.07	0.23 ± 0.07	0.98
	MALDI−CHCA	25.6	1.18 ± 0.13	0.33 ± 0.10	0.98
picosecond	DIOS−PFP	60.4	1.83 ± 0.11	0.23 ± 0.14	0.94
	SiNW−PFP	6.67	1.26 ± 0.06	0.19 ± 0.05	0.98
	MALDI−CHCA	45.2	0.70 ± 0.41	0.41 ± 0.16	0.99

and DIOS from a PFP-derivatized surface. These internal energy distributions do not account for the kinetic shift associated with our experimental setup. Nevertheless, the distributions are meaningful in a relative sense and can be used to compare the different methods.

Together with the selected fluence, F, the characteristic parameters of the internal energy distributions, the mean value, E^*, the width, ΔE, and the squared correlation coefficients, R^2, are listed in Table 1. The correlation coefficients are remarkably high (>0.91) indicating that the data is statistically consistent with the model function. Because of the much lower fluence range utilized for the SiNW systems, no consensus fluence value was found with the other two methods. What can be compared are the distributions at fluence levels selected close to the ion-generation threshold for the individual methods. From a practical perspective, this is a meaningful comparison because in all SLDI methods the best signal quality is achieved at close to threshold conditions.

An inspection of the mean values of the distributions in Table 1 indicates that MALDI from CHCA matrix with picosecond laser excitation results in ions with the lowest internal energy. The MALDI data with the nanosecond laser points to significantly higher internal energy. Both nanosecond and picosecond laser excitation produce ions from SiNW substrates with mean internal energies comparable to nanosecond MALDI. The mean internal energy values are significantly higher for DIOS than either for MALDI or for SiNWs. These results are consistent with our earlier observation for the 4M thermometer ions. Here we see that the internal energies of ions desorbed from SiNWs are comparable (for the nanosecond laser) or even higher (for the picosecond laser) than from MALDI. This is despite the 5−8 times lower fluence requirement of the SiNW process. It is also noteworthy that in desorption from SiNWs the nanosecond and picosecond excitation produce very similar internal energy distributions.

Both the means and the widths of the internal energy distributions in Figure 5 can be linked to in-plume processes. These include collisional energy transfer but also the interaction of the laser pulse with the plume. For both lasers, SiNWs produce ions with the narrowest energy distributions of the three methods. In relation to MALDI, this means that the produced plume in desorption from SiNWs is significantly less dense; thus, in-plume collisional energy transfer is limited. In comparison with DIOS, the SiNWs produce narrower distributions because of the lack of plume confinement and associated collisional dispersion that occurs in the nanopores of porous silicon.

A comparison of the distributions in Figure 5 for the two different lasers in the three methods reveals that the desorption from SiNWs is effected the least by laser pulse length. For this SLDI method, when the nanosecond excitation source is replaced by a picosecond laser, both the mean and the width of the internal energy distributions remain practically unchanged (see Table 1). In MALDI from the CHCA matrix, however,

there is a large ~0.5 eV difference in the mean values between the two pulse lengths. In this case, the nanosecond laser produces ions with larger internal energy because the energy deposition by the laser into the matrix molecules continues in the gas phase (optically thick plume). Because of the high plume density, the deposited energy is efficiently communicated to the thermometer ions. The width of the distribution, however, only changes by 0.08 eV which is within experimental error.

In DIOS, the order is reversed and the difference in the means of the distributions is reduced. Here, the nanosecond laser produces ions with ~0.2 eV lower internal energy. The width of the distribution changes by 0.14 eV, from 0.37 eV for the nanosecond laser to 0.23 eV for the picosecond laser. This change is also within experimental error.

It is interesting to note that the picosecond laser accentuates the differences in internal energies between the three methods. In other words, picosecond laser excitation makes desorption in MALDI considerably more and DIOS slightly less soft. A similar trend was found for the primary ionization of CHCA and other two common MALDI matrixes, 2,5-dihydroxybenzoic acid and sinapinic acid.[33] In the entire fluence range, the molecular ion yield for all three matrixes was significantly higher for the picosecond laser.

Conclusions

Because of the excellent spectrum quality and the simplicity of sample preparation, SLDI of large ions from nanostructures is gaining importance. Understanding the correlation between the features of these structures and the desorption mechanism benefits fundamental studies and applications alike. Even the effect of simple morphological parameters, such as the size of individual nanoscopic features, their morphology, and in the case of periodic structures, their periodicity, on the ion yields is unclear. We only have a limited understanding of the important material properties and laser light characteristics. The factors that are at play can change between different structure types.

This study focused on the internal energy transfer in SLDI from SiNWs and its relationship to nanoporous silicon in DIOS and to conventional MALDI. The use of preformed thermometer ions enabled us to explore the effect of desorption on internal energy transfer separately from the influence of ionization. The confinement of thermal energy in SiNWs resulted in a very low fluence requirement to reach high surface temperatures and consequently achieve desorption.

The radical difference in morphology between nanowires (SiNW) and nanopores (DIOS) also shed light on the link between plume confinement and energy transfer. In DIOS, the quasi-one-dimensional expansion in the nanopores sustained relatively high plume pressure and thereby promoted energy transfer. The plume expansion in desorption from SiNWs is almost unimpeded and more three-dimensional in nature. Thus, the plume density drops rapidly and the energy transfer to the thermometer ions is more limited. Further desorption/ionization experiments with controlled morphology are needed to gain additional insight into the understanding of mechanisms involved in SLDI from these nanostructures.

Luo et al.

References and Notes

(1) Tanaka, K.; Kaki, H.; Ido, Y.; Akita, S.; Yoshida, Y.; Yoshida, T. *Rapid Commun. Mass Spectrom.* **1988**, *2*, 151−153.

(2) Schurenberg, M.; Dreisewerd, K.; Hillenkamp, F. *Anal. Chem.* **1999**, *71*, 221−229.

(3) Sunner, J.; Dratz, E.; Chen, Y. C. *Anal. Chem.* **1995**, *67*, 4335−4342.

(4) Han, M.; Sunner, J. *J. Am. Soc. Mass Spectrom.* **2000**, *11*, 644−649.

(5) Kinumi, T.; Saisu, T.; Takayama, M.; Niwa, H. *J. Mass Spectrom.* **2000**, *35*, 417−422.

(6) McLean, J. A.; Stumpo, K. A.; Russell, D. H. *J. Am. Chem. Soc.* **2005**, *127*, 5304−5305.

(7) Xu, S.; Li, Y.; Zou, H.; Qiu, J.; Guo, Z.; Guo, B. *Anal. Chem.* **2003**, *75*, 6191−6195.

(8) Ren, S.; Zhang, L.; Cheng, Z.; Guo, Y. *J. Am. Soc. Mass Spectrom.* **2005**, *16*, 333−339.

(9) Cuiffi, J. D.; Hayes, D. J.; Fonash, S. J.; Brown, K. N.; Jones, A. D. *Anal. Chem.* **2001**, *73*, 1292−1295.

(10) Wei, J.; Buriak, J. M.; Siuzdak, G. *Nature* **1999**, *399*, 243−246.

(11) Kraj, A.; Dylag, T.; Gorecka-Drzazga, A.; Bargiel, S.; Dziuban, J.; Silberring, J. *Acta Biochim. Pol.* **2003**, *50*, 783−787.

(12) Thomas, J. J.; Shen, Z. X.; Crowell, J. E.; Finn, M. G.; Siuzdak, G. *Proc. Natl. Acad. Sci. U.S.A.* **2001**, *98*, 4932−4937.

(13) Arakawa, R.; Shimomae, Y.; Morikawa, H.; Ohara, K.; Okuno, S. *J. Mass Spectrom.* **2004**, *39*, 961−965.

(14) Shen, Z. X.; Go, E. P.; Gamez, A.; Apon, J. V.; Fokin, V.; Greig, M.; Ventura, M.; Crowell, J. E.; Blixt, O.; Paulson, J. C.; Stevens, R. C.; Finn, M. G.; Siuzdak, G. *ChemBioChem* **2004**, *5*, 921−927.

(15) Bhattacharya, S. H.; Raiford, T. J.; Murray, K. K. *Anal. Chem.* **2002***, 74*, 2228−2231.

(16) Go, E. P.; Apon, J. V.; Luo, G.; Saghatellian, A.; Daniels, R. H.; Sahi, V.; Dubrow, R.; Cravatt, B. F.; Vertes, A.; Siuzdak, G. *Anal. Chem.* **2005**, *77*, 1641−1646.

(17) Cui, Y.; Lauhon, L. J.; Gudiksen, M. S.; Wang, J. F.; Lieber, C. M. *Appl. Phys. Lett.* **2001**, *78*, 2214−2216.

(18) Yorikawa, H.; Uchida, H.; Muramatsu, S. *J. Appl. Phys.* **1996**, *79*, 3619−3621.

(19) Zhao, X.; Wei, C. M.; Yang, L.; Chou, M. Y. *Phys. Rev. Lett.* **2004**, *92*, 236805.

(20) Li, D.; Wu, Y.; Kim, P.; Shi, L.; Yang, P.; Majumdar, A. *Appl. Phys. Lett.* **2003**, *83*, 2934−2936.

(21) Zou, J.; Balandin, A. *J. Appl. Phys.* **2001**, *89*, 2932−2938.

(22) Sadeghi, M.; Vertes, A. *Appl. Surf. Sci.* **1998**, *127−129*, 226−234.

(23) Joshi, A. A.; Majumdar, A. *J. Appl. Phys.* **1993**, *74*, 31−39.

(24) Chen, G. *Phys. Rev. Lett.* **2001**, *86*, 2297−2300.

(25) Collettte, C.; Drahos, L.; De Pauw, E.; Vekey, K. *Rapid Commun. Mass Spectrom.* **1998**, *12*, 1673−16778.

(26) Drahos, L.; Heeren, R. M. A.; Collette, C.; De Pauw, E.; Vekey, K. *J. Mass Spectrom.* **1999**, *34*, 1373−1379.

(27) Mowry, C. D.; Johnston, M. V. *J. Phys. Chem.* **1994**, *98*, 1904−1909.

(28) Stevenson, E.; Breuker, K.; Zenobi, R. *J. Mass Spectrom.* **2000**, *35*, 1035−1041.

(29) Luo, G.; Marginean, I.; Vertes, A. *Anal. Chem.* **2002**, *74*, 6185−6190.

(30) Vertes, A.; Luo, G.; Ye, L.; Chen, Y.; Marginean, I. *Appl. Phys. A* **2004**, *79*, 823−825.

(31) Derwa, F.; De Pauw, E.; Natalis, P. *Org. Mass Spectrom.* **1991**, *26*, 117−118.

(32) Alimpiev, S.; Nikiforov, S.; Karavanskii, V.; Minton, T.; Sunner, J. *J. Chem. Phys.* **2001**, *115*, 1891−1901.

(33) Chen, Y.; Vertes, A. *J. Phys. Chem. A.* **2003**, *107*, 9754−9761.

(34) Luo, G.; Chen, Y.; Siuzdak, G.; Vertes, A. *J. Phys. Chem. B* **2005**, *109*, 24450−24456.

(35) Stockbauer, R. *J. Chem. Phys.* **1973**, *58*, 3800−3815.